Materials Science and Engineering, A155 (1992) 147–158

Mechanical behavior and interface design of $MoSi_2$-based alloys and composites

R. Gibala*, A. K. Ghosh, D. C. Van Aken, D. J. Srolovitz, A. Basu, H. Chang, D. P. Mason and W. Yang

Department of Materials Science and Engineering, The University of Michigan, Ann Arbor, MI 48109-2136 (USA)

Abstract

The mechanical behavior of hot pressed $MoSi_2$-based composites containing Mo_5Si_3, SiO_2, CaO and TiC as reinforcing second phases was investigated in the temperature regime 1000–1300 °C. The effects of strain rate on the flow stress for Mo_5Si_3-, SiO_2- and CaO-containing composites are presented. Effects of several processing routes and microstructural modifications on the mechanical behavior of $MoSi_2$–Mo_5Si_3 composites are given. Of these four composite additions, Mo_5Si_3 and CaO produce strengthening of $MoSi_2$ in the temperature range investigated. SiO_2 greatly reduces the strength, consistent with the formation of a glassy phase at interface and interphase boundaries. TiC reduces the flow stress of $MoSi_2$ in a manner that suggests dislocation pumping into the $MoSi_2$ matrix. The strain rate effects indicate that dislocation creep (glide and climb) processes operate over the temperature range investigated, with some contribution from diffusional processes at the higher temperatures and lower strain rates. Erbium is found to be very effective in refining the microstructures and in increasing the hardness and fracture properties of $MoSi_2$-Mo_5Si_3 eutectics prepared by arc melting. Initial results on microstructural modeling of the deformation and fracture of $MoSi_2$-based composites are also reported.

1. Introduction

There is increasing need for high-strength, oxidation-resistant materials for elevated temperature structural applications, particularly in aircraft gas turbines and spacecraft air frames. The silicides of refractory metals such as molybdenum, tungsten, niobium and tantalum have great potential as the matrix materials for new composites with service capabilities at temperatures above approximately 1200 °C. In particular, $MoSi_2$, which melts at 2030 °C, exhibits excellent high-temperature oxidation resistance because of the formation of a protective silica film and has already been used effectively as the major constituent in super kanthal (an $MoSi_2$–SiO_2 alloy) furnace windings for applications to temperatures as high as 1800 °C. The major problems in the use of $MoSi_2$ for load-bearing structural applications have been inadequate high temperature strength at significant applied stresses above 1200 °C and poor fracture toughness below the ductile-to-brittle transition temperature (DBTT) of approximately 1000 °C. Above 1000 °C, $MoSi_2$ yields plastically and deforms by dislocation motion similar to the behavior of metallic materials. The need for composite and alloy additions for strengthening at temperatures above 1200 °C and for similar or alternative additions for toughening at lower temperatures has led to extensive investigation of $MoSi_2$ in the past few years [1].

The purpose of our research is to investigate promising composite approaches to obtain a more fundamental understanding of the mechanical behavior of $MoSi_2$ and $MoSi_2$-based composites at both ambient and elevated temperatures. In the present investigation, we report on the effects of several different single composite additions, including Mo_5Si_3, SiO_2, CaO and TiC, all in particulate form. Mo_5Si_3 was investigated as an elastically hard, strong, brittle second phase which can potentially strengthen $MoSi_2$ at high temperatures and impart low temperature toughness by crack deflection processes. SiO_2 was investigated in small part because of its use in the manufacture of super kanthal, but more importantly because of the role of silica as an interface and interphase contaminant during the processing of $MoSi_2$ and $MoSi_2$-based composites, which leads to extensive boundary sliding at elevated temperatures. Both of these additions have lower coefficients of thermal expansion (CTE) than $MoSi_2$ (see Table 1) and thus are capable of generating tensile residual stresses in the hoop direction in the matrix after fabrication and cooling to room temperature. Residual stresses in the radial direction are compressive in nature and are benign from the standpoint of crack generation. CaO

*Present address: Center for Materials Science, Los Alamos National Laboratory, Los Alamos, NM 87545, USA.

0921-5093/92/$5.00

TABLE 1. Coefficients of thermal expansion (CTE) and melting temperatures T_m for $MoSi_2$ and several potential particulate additions

Material	CTE ($°C^{-1}$) @ 1000 °C	T_m (°C)
$MoSi_2$	8.5×10^{-6}	2030
TiC	7.7×10^{-6}	3250
Mo_5Si_3	6.7×10^{-6} (@ 500 °C)	2180
HfC	6.25×10^{-6}	3890
HfB_2	5.5×10^{-6}	3250
SiO_2 (vitreous)	0.55×10^{-6}	1710
CaO	13.1×10^{-6}	2570
MgO	15.7×10^{-6}	2800
Ce_2O	14×10^{-6}	2600

was examined as a more stable addition that might reduce boundary sliding. The CTE of CaO is large compared with that of $MoSi_2$, which allows analysis of effects of thermally induced residual stresses. TiC, with a melting temperature above 3000 °C, offers the unique prospect of having higher strength than $MoSi_2$ at low temperatures but comparable or somewhat lower strength and higher plasticity at temperatures near and above the DBTT. The CTE of TiC is approximately the same as that of $MoSi_2$. These results serve as experimental data with which we can compare parallel attempts to model the deformation and fracture behavior of composite microstructures and to develop methods by which the controlling microstructural parameters and physical properties can be optimized. An initial report of these modeling methods and their results is included.

2. Experimental details

2.1. Fabrication of materials

$MoSi_2$. For most experiments, the monolithic $MoSi_2$ was prepared from as-received powders screened to −325 mesh obtained from Cerac, Incorporated. The powders were hot pressed at 1700 °C under 25–30 MPa pressure for 1–2 h in grafoil-lined graphite dies and an argon atmosphere. The typical grain size (d) of $MoSi_2$ after such treatment was 30 μm. The processing schedule for $MoSi_2$ was always identical with that used for the $MoSi_2$-based composite being compared. In some selected experiments on $MoSi_2$–Mo_5Si_3 eutectics, the monolithic material and eutectics of various volume fractions of Mo_5Si_3 were prepared by arc melting under an argon atmosphere. The densities of the hot-pressed $MoSi_2$ specimens were in the range 94%–96%. Porosity in arc-melted $MoSi_2$ was larger and depended on the exact solidification conditions. Densities ranged from 70%–85%. In some experiments, post-solidification hot isostatic pressing was used to reduce the range and total amount of porosity observed in arc-melted materials.

$MoSi_2$–Mo_5Si_3 composites. Most of the $MoSi_2$-based composites containing Mo_5Si_3 in the range 15–30 vol.% were made by slurry milling mixtures of the $MoSi_2$ matrix and molybdenum reinforcement powders (−325 mesh) for periods of at least 24 h. The mixtures were hot pressed at 1700 °C at 25 MPa for 2 h. This treatment was sufficient to form the $MoSi_2$–Mo_5Si_3 eutectic mixture in the equilibrium proportions of 15%–30% expected from the phase diagram. In some experiments, the eutectic mixtures were prepared by arc melting $MoSi_2$ and molybdenum powders followed either by hot pressing or hot isostatic pressing. These were done at 1700 °C at 25–28 MPa for 1.5–2 h. Some arc-melted eutectics were also crushed to produce powder and subsequently hot pressed to produce materials with potentially less silica at interface or interphase boundaries. Erbium was added to some arc-melted eutectics as a potential microstructural refiner and as an additional means of removing oxygen from the melt in experiments based on solidification methods.

$MoSi_2$–SiO_2 composites. These composites which contained approximately 15 vol.% silica were obtained as a commercial super kanthal. The composites were typically 94% dense.

$MoSi_2$–CaO composites. The $MoSi_2$–CaO composites were made by ball milling CaO and $MoSi_2$ powders of −325 mesh for 24 h and then hot pressing the mixtures at 1700 °C at 25 MPa pressure for 2 h. The CaO powder was obtained from Johnson Matthey, Incorporated. The hot-pressed composites of 20 vol.% CaO were 95% dense.

$MoSi_2$–TiC composites. $MoSi_2$–10vol.%TiC composites were prepared by dry blending in a ball mill for 20 h prior to hot pressing at 1700 °C at 30 MPa for 1 h. The TiC was obtained from Johnson Matthey, Incorporated as 2.5–4 μm size powder with the stoichiometry of $TiC_{0.95}$. The hot-pressed composite was approximately 95% dense. The TiC particles were well distributed through the matrix, but because of agglomeration the final particle sizes varied from 5 to 60 μm, with a mean value of 10 μm.

2.2. Microstructural characterization

Monolithic and composite microstructures were examined by light optical, scanning and transmission electron microscopies (SEM and TEM). Optical and SEM methods were used to assess grain and second-

phase structure, shape and distribution before and after deformation. TEM was used to characterize the composite substructures in more detail, including analysis of dislocation substructures and phase boundary structures by high-resolution TEM (HRTEM). Conventional TEM studies were done on a JEOL 2000FX microscope, while HRTEM observations were done on a JEOL 4000EX microscope.

2.3. Mechanical properties

Microhardness indentation techniques were used to evaluate the temperature dependence of the strength of monolithic $MoSi_2$ and the several composites investigated, as well as the behavior of some of the composite additions. Hot hardness testing was done at temperatures of 25–1300 °C with a Nikon QM-2 hot hardness tester. Diamond Vickers indentations at a load of 1 kgf (9.8 N) were used in most experiments.

Most mechanical testing was done in compression at a constant crosshead speed corresponding to an initial strain rate of 10^{-4} s^{-1} on specimens of dimensions $6 \times 3 \times 3$ mm^3. All tests were done in air at temperatures up to 1300 °C. Yttria was used as a platen lubricant to minimize friction. Step-strain rate experiments at 10^{-6}–10^{-3} s^{-1} were also performed on most composites at several temperatures in the range 1000–1300 °C to determine stress exponents and activation energies for deformation. Most specimens were cut from the hot-pressed compacts or arc-melted and/or hot isostatically pressed ingots using a diamond saw. Compression samples of $MoSi_2$–SiO_2 alloys were cut from 3 mm diameter super kanthal heating elements.

3. Results and discussion

3.1. $MoSi_2$

The monolithic $MoSi_2$ prepared by hot pressing exhibited microstructures and mechanical properties similar to those reported previously by other investigators [1, 2]. The typical microstructure of the as-processed material is given in Fig. 1. Regular equiaxed grain sizes of 25–35 μm and densities of $95 \pm 1\%$ with mainly fine dispersed porosity in the range of a few to several micrometers in diameter were observed. Deformation had little or no effect on the microstructure given in Fig. 1 except at the higher temperatures and lowest strain rates examined, where dynamic grain growth occurred during mechanical testing. Dislocation substructures and dislocation types were much the same as those reported by Umakoshi *et al.* [3] and Unal *et al.* [4]. Specifically, dislocations with Burgers vectors $\langle 100 \rangle$, $\langle 110 \rangle$ and $\frac{1}{2}\langle 111 \rangle$ were observed in specimens deformed at 1300 °C. At 900 °C $\frac{1}{2}\langle 331 \rangle$ dislocations were found [5].

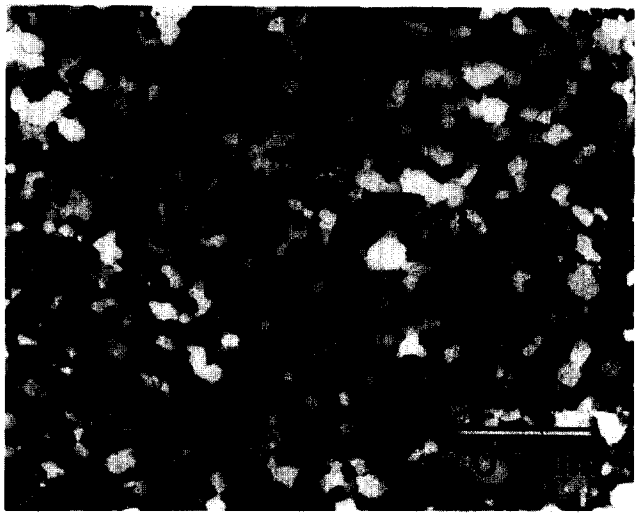

Fig. 1. Grain structure in polarized light of as-hot-pressed $MoSi_2$, hot pressed at 1700 °C for 1 h under 29.4 MPa. The average grain size is 30 μm.

The mechanical properties of the monolithic $MoSi_2$ and the various $MoSi_2$-based composites are given in Figs. 2–7. The results are presented in the form of compressive flow stress–strain rate data obtained from step-strain rate experiments (Figs. 2–4), selected elevated temperature compressive stress–strain curves (Fig. 5), and hot hardness data for the $MoSi_2$ and selected reinforcements and composites (Figs. 6 and 7). At 1200 °C, the compressive flow stress of $MoSi_2$ ranges from about 300–340 MPa at a strain rate $\dot{\varepsilon}$ of 10^{-4} s^{-1} to about 75 MPa at $\dot{\varepsilon} = 10^{-6}$ s^{-1}. The corresponding stress exponent n varies from 5 to 2–2.5 over the same range of strain rates. At 1100 °C, the compressive flow stress is about 420 MPa at $\dot{\varepsilon} = 10^{-4}$ s^{-1} and falls to 160 MPa at $\dot{\varepsilon} = 10^{-6}$ s^{-1}. The stress exponent changes from about 8 to 3 over this same range of strain rates [6]. The implication is that dislocation creep, with both glide and climb contributions, dominates at these temperatures and strain rates. Glide processes dominate at the lower temperatures and higher strain rates, and diffusional creep may contribute in addition to climb at the higher temperatures and lower strain rates.

In the stress–strain curves of Fig. 5, $MoSi_2$ exhibits significant apparent work hardening, but we have not yet unambiguously sorted out the relative contributions of plastic flow and cracking in these materials as a function of strain. The temperature dependence of the hardness of $MoSi_2$ up to 1300 °C given in Fig. 6 is much more gradual than that typically reported for the yield strength, probably because microhardness does not sample a sufficient volume of material to be affected as much by the rapidly decreasing viscosity of the glassy silica grain boundary phase with increasing

temperature to the same extent as uniaxial compression or bend tests of bulk materials. The typical indentation width along the major axis at 1 kgf is 50–80 μm over the temperature range 25–1300 °C compared with the typical grain size of 30 μm.

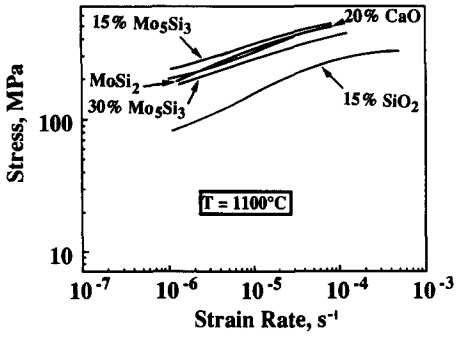

Fig. 2. Flow stress as a function of strain rate as determined from decremental step-strain rate test in compression conducted on $MoSi_2$-based composites at 1100 °C.

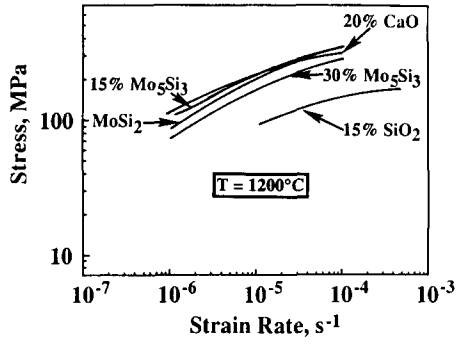

Fig. 3. Flow stress as a function of strain rate as determined from decremental step-strain rate test in compression conducted on $MoSi_2$-based composites at 1200 °C.

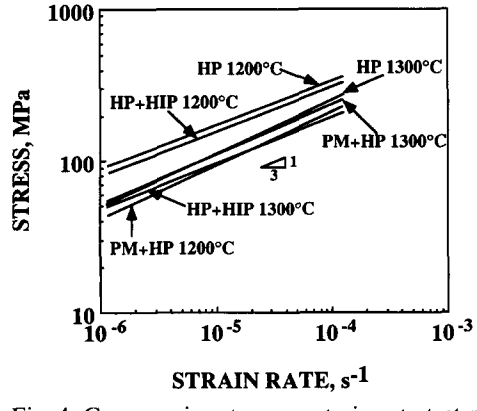

Fig. 4. Compressive stress *vs.* strain rate test results for $MoSi_2$-45vol.%Mo_5Si_3 samples processed by hot pressing arc-melted buttons (HP), hot-pressed and hot isostatically pressed arc-melted buttons (HP + HIP) and arc-melted buttons which were crushed to produce powder and subsequently hot pressed (PM + HP). Note that the stress exponent is approximately 3 for all processing paths at 1200 °C and 1300 °C.

3.2. $MoSi_2$–Mo_5Si_3 composites

The microstructure of the hot-pressed $MoSi_2$–Mo_5Si_3 particulate composites is typified by the micrographs for the 30 vol.% composite given in Fig. 8. The $MoSi_2$ matrix in the as-processed state maintains the

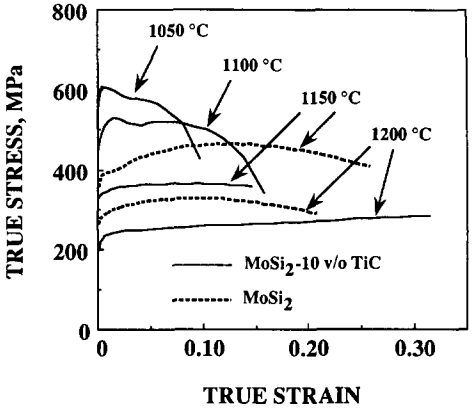

Fig. 5. True stress *vs.* true strain in compression for $MoSi_2$ and $MoSi_2$–10vol.%TiC. The initial strain rate in the constant crosshead speed tests is 10^{-4} s^{-1}.

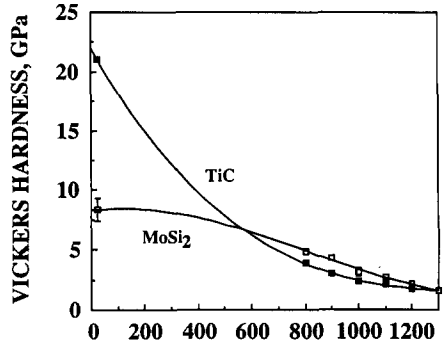

Fig. 6. Vickers hardness *vs.* temperature for $MoSi_2$ and TiC tested as separate specimens.

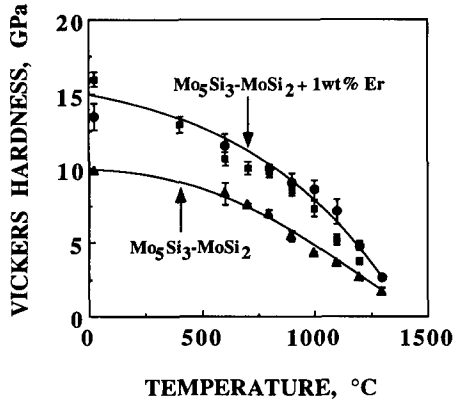

Fig. 7. Hot hardness tests of the erbium-modified and untreated eutectic alloys. Results show an increased hardness for erbium-modified alloys.

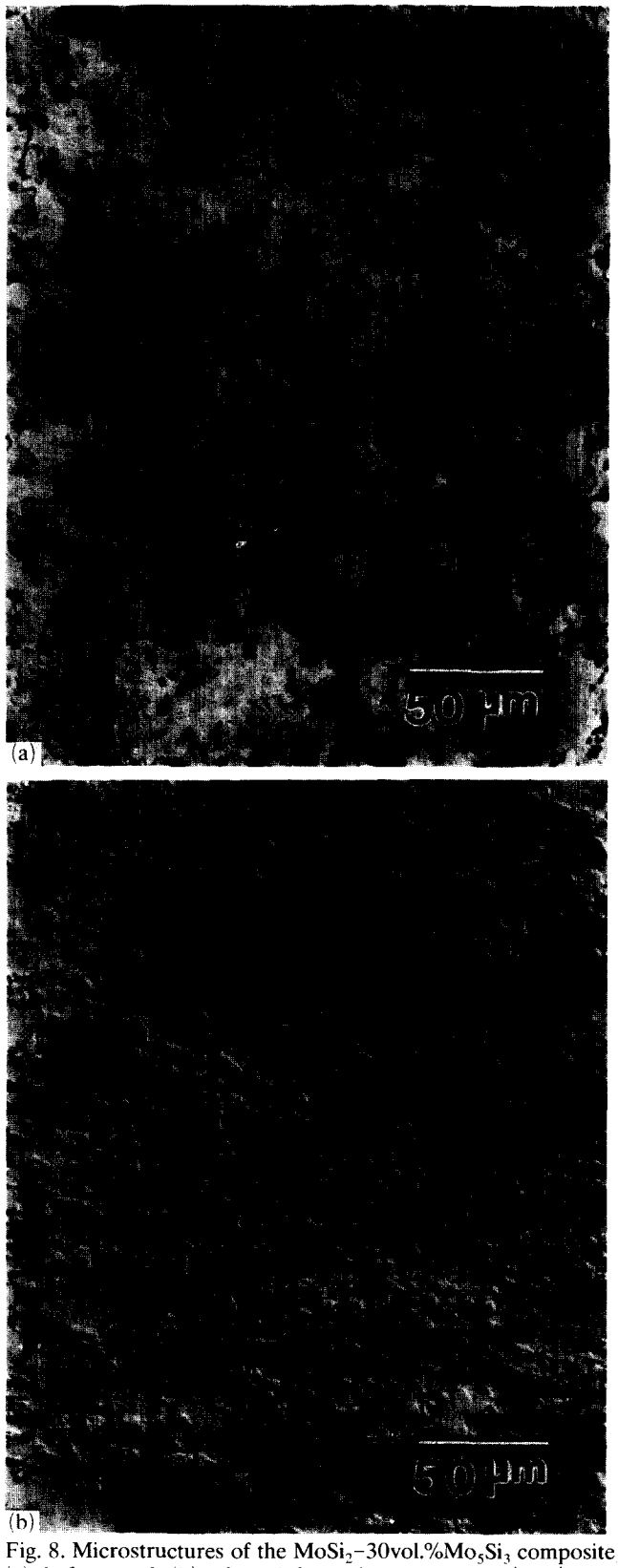

Fig. 8. Microstructures of the $MoSi_2$–30vol.%Mo_5Si_3 composite (a) before and (b) after deformation at $\dot{\varepsilon} = 10^{-4}$ s^{-1} and $T = 1200$ °C. Dynamic grain refinement of the matrix in the vicinity of Mo_5Si_3 is observed in (b) (phase identification, A $MoSi_2$, B Mo_5Si_3): (a) $\varepsilon = 0$, $d = 29$ μm; (b) $\varepsilon = 0.81$, $d = 25$ μm and $d = 7.5$ μm.

same 30 μm grain size and equiaxed shape given for the monolithic material in Fig. 1. The Mo_5Si_3 exists in relatively large regions and is irregularly distributed in the matrix. Upon deformation at 1200 °C and $\dot{\varepsilon} = 10^{-4}$ s^{-1}, the Mo_5Si_3 breaks up into much smaller particles, and the $MoSi_2$ matrix nearest these particles has developed into a grain structure of about 8 μm in average grain size. This microstructure constitutes about two thirds of the total area fraction. The remainder of the matrix microstructure consists of larger, slightly elongated grains of $MoSi_2$ with an average intercept of 25 μm.

The mechanical behavior of the hot-pressed $MoSi_2$–Mo_5Si_3 particulate composites at 1100 °C and 1200 °C is given in Figs. 2 and 3 respectively, along with data for other hot-pressed particulate composites. The compressive yield stress decreases with a decrease in strain rate and an increase in temperature for all composites. The addition of 15 vol.% Mo_5Si_3 increases the strength of $MoSi_2$ at all strain rates, but increasing the volume fraction of Mo_5Si_3 to 30% decreases the strength to values below that observed for the monolithic material over all strain rates and temperatures investigated. The strengthening of $MoSi_2$ by 15 vol.% is less at 1200 °C than at 1100 °C, but it is still significant at the lower strain rates.

Although the strength of Mo_5Si_3 is greater than that of $MoSi_2$, the expected strengthening in these composites due to Mo_5Si_3 is not observed. The most probable explanation lies in the dynamic grain refinement, illustrated in part in Fig. 8, which increases with increasing strain and is especially large for the 30% Mo_5Si_3 composite. The presence of smaller grains enhances the rate of dislocation climb and other diffusional creep processes and can produce both the small strengthening effect observed for the 15% Mo_5Si_3 composite and the reduced strength of the 30% Mo_5Si_3 composite. The values of the stress exponent n obtained from Figs. 2 and 3 are consistent with this explanation. The stress exponent for the 15% Mo_5Si_3 composite at 1200 °C falls from about 11 at $\dot{\varepsilon} = 10^{-4}$ s^{-1} to 2.5 at $\dot{\varepsilon} = 10^{-6}$ s^{-1}. At 1100 °C, n falls from about 8 to 5–6 over the same range of strain rates. At 1000 °C, n was in the range 18–11 over these same strain rates. However, n was much smaller for the 30% Mo_5Si_3 composites: 5–2.5 for $\dot{\varepsilon} = 10^{-4}$ to 10^{-6} s^{-1} at 1200 °C and 6–5 for $\dot{\varepsilon} = 10^{-4}$ to 10^{-6} s^{-1} at 1100 °C [6]. Thus, the overall small values of n, the low flow stresses, and the very substantial dynamic grain refinement of the 30% Mo_5Si_3 composite suggest that the strength of the $MoSi_2$–Mo_5Si_3 composites is controlled by grain size effects over a wide range of temperatures and strain rates and is not influenced significantly by other softening processes. The significant strengthening at the lower strain rates for the 15% Mo_5Si_5 composite is

probably associated with the breakdown of the larger particles during deformation. The smaller particles then act to hinder dislocation motion in the manner expected for small particle dispersion strengthening at elevated temperatures.

Similar investigations on $MoSi_2$–Mo_5Si_3 composites were carried out on arc-melted materials with microstructures of the type illustrated in Fig. 9. These materials are near the eutectic composition and contain Mo_5Si_3 as a script microstructure, which can be substantially refined by the addition of small amounts (1 wt.%) of erbium. Microalloying with erbium was also investigated as a means of reducing the oxygen concentration in the eutectic material by acting as a gettering agent and removing oxygen from the melt. The presence of rare-earth oxides may also contribute to the creep strength of the eutectic microstructure. The microstructure of Fig. 9 illustrates two effects of erbium additions: the scale of the script microstructure is reduced and the occurrence of pro-eutectic $MoSi_2$ is greatly diminished. Erbium-rich particles are present in the observed microstructures as inclusions associated with the Mo_5Si_3 phase (B in Fig. 9). Microprobe analysis reveals that these particles are rich in oxygen compared with either silicide phase. The volume fraction of Mo_5Si_3 is larger than that obtained in hot-pressed $MoSi_2$–Mo_5Si_3 composites of Figs. 2, 3 and 8, of order 45% for the materials illustrated in Fig. 9.

Mechanical behavior data for the arc-melted $MoSi_2$–Mo_5Si_3 composites are given in Figs. 4 and 7. Figure 4 gives compressive flow stress–strain rate results similar to those presented for the hot-pressed particulate composites in Figs. 2 and 3. Data at 1200 °C and 1300 °C are presented for arc-melted alloys which were processed by hot pressing (HP), by hot pressing and hot isostatic pressing (HP + HIP), and by crushing to produce powder and subsequent hot pressing (PM + HP). There is no systematic difference in the strength effected by these three processing routes in the results obtained at 1300 °C. At 1200 °C, the HP and HP + HIP materials are consistently stronger than the PM + HP composites. All three sets of materials appear to be characterized by a stress exponent of approximately 3 at both temperatures, consistent with many of those obtained for the hot-pressed particulate materials of Figs. 2 and 3. The strengths appear to be somewhat lower than the hot-pressed particulate materials in Figs. 2 and 3, but consistent with possible effects of the larger volume fraction of Mo_5Si_3. We have not yet compared detailed $MoSi_2$ matrix microstructures and properties between the hot-pressed and arc-melted materials as a source of these strength differences.

The effects of erbium modification on the mechanical properties of the arc-melted eutectic composite

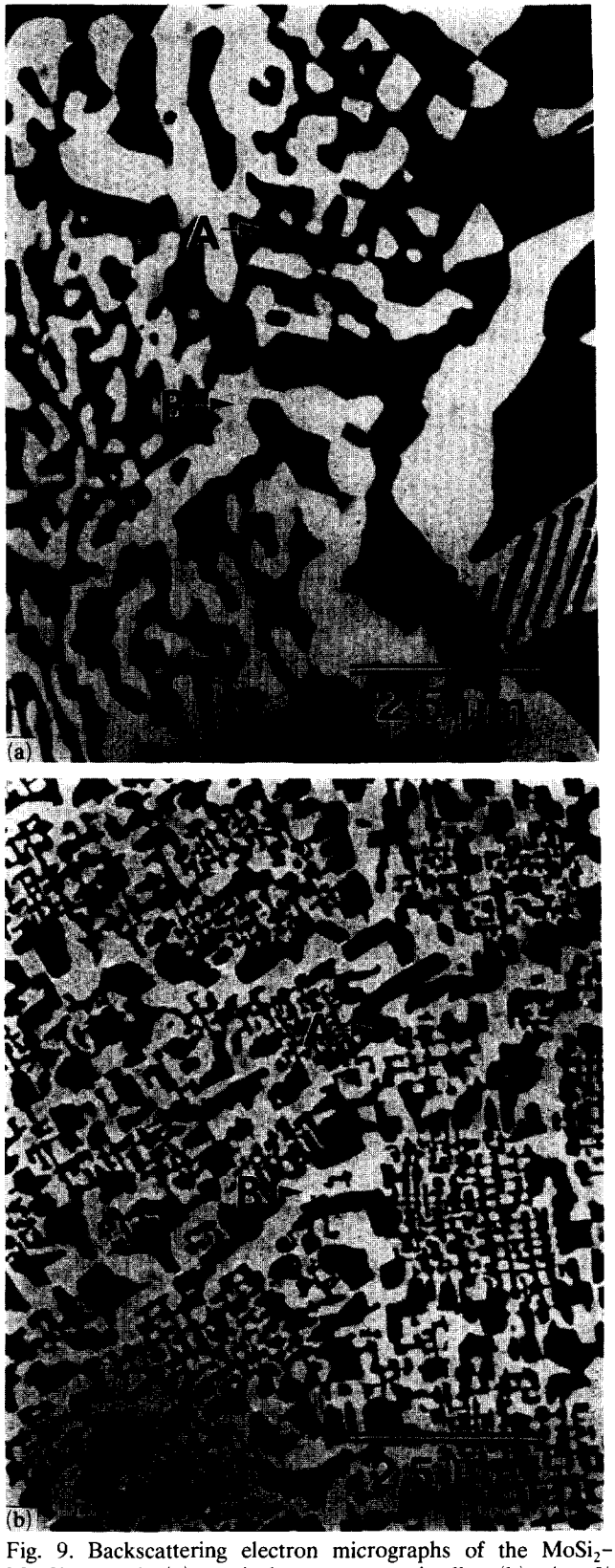

Fig. 9. Backscattering electron micrographs of the $MoSi_2$–Mo_5Si_3 eutectic: (a) a typical arc-cast eutectic alloy; (b) a 1 wt.% Er modified eutectic alloy. Note the microstructural refinement with the addition of erbium. An erbium-rich phase appears as bright particles within the Mo_5Si_3 phase (phase identification, A $MoSi_2$, B Mo_5Si_3).

were examined by hot hardness testing methods, as illustrated in Fig. 7. The erbium-treated material was found to have a substantially higher hardness at all temperatures from 25 °C to 1300 °C. This increase in hardness is probably due to the increased constraint placed on the $MoSi_2$ matrix by the Mo_5Si_3 as the microstructure becomes more refined. At high temperatures, the increased constraint has its origin in the reduced mean free path of dislocations in the $MoSi_2$ phase effected by the finer two-phase microstructure. At low temperatures, crack deflection processes are more effective in the finer microstructure. There may also be a residual solid solution strengthening effect and additional strengthening associated with the erbium-based oxide particles present in the Mo_5Si_3 phase. These effects will be sorted out in future experiments.

The microstructural refinement resulting from the addition of erbium most likely occurs from a decrease in the interfacial surface energy and a subsequent change in the solidification mechanism. Similar results have been observed in rare-earth-modified Al–Si eutectics [7]. We speculate at this point that the microstructural refinement results from oxygen gettering by erbium and that removal of these interstitials may improve the fracture characteristics of such $MoSi_2$–Mo_5Si_3 composite microstructures. Our initial studies to investigate the fracture characteristics have been limited to use of room temperature hardness indentations to observe the extent of cracking and the resulting crack paths in erbium-modified and untreated eutectic alloys. We have found that the crack path is deflected around the finer Mo_5Si_3 particles of the erbium-modified alloys and that these alloys are not as extensively cracked as the untreated alloys. Thus, it may be possible to improve the fracture toughness by microstructural refinement, but we have not yet shown that such improvement is a direct result of microalloying.

3.3. $MoSi_2$–SiO_2 composites

The microstructure of the super kanthal used in this study is shown in Fig. 10. It consists of 1–20 μm discrete particles of SiO_2 located at the grain boundaries of the $MoSi_2$ matrix which has an average grain size of about 30 μm. During deformation at 1100–1200 °C, the soft SiO_2 is squeezed along and between the grain boundaries of the matrix, as illustrated by arrows in Fig. 10(b). The effect on the mechanical properties is very large. In Figs. 2 and 3, the strength of the $MoSi_2$–SiO_2 composite at 1100 °C and 1200 °C respectively, is well below that of any other composite and the monolithic material. The stress exponent is in the range 2.5–5 at all strain rates investigated at both temperatures and does not change much as a function of strain rate.

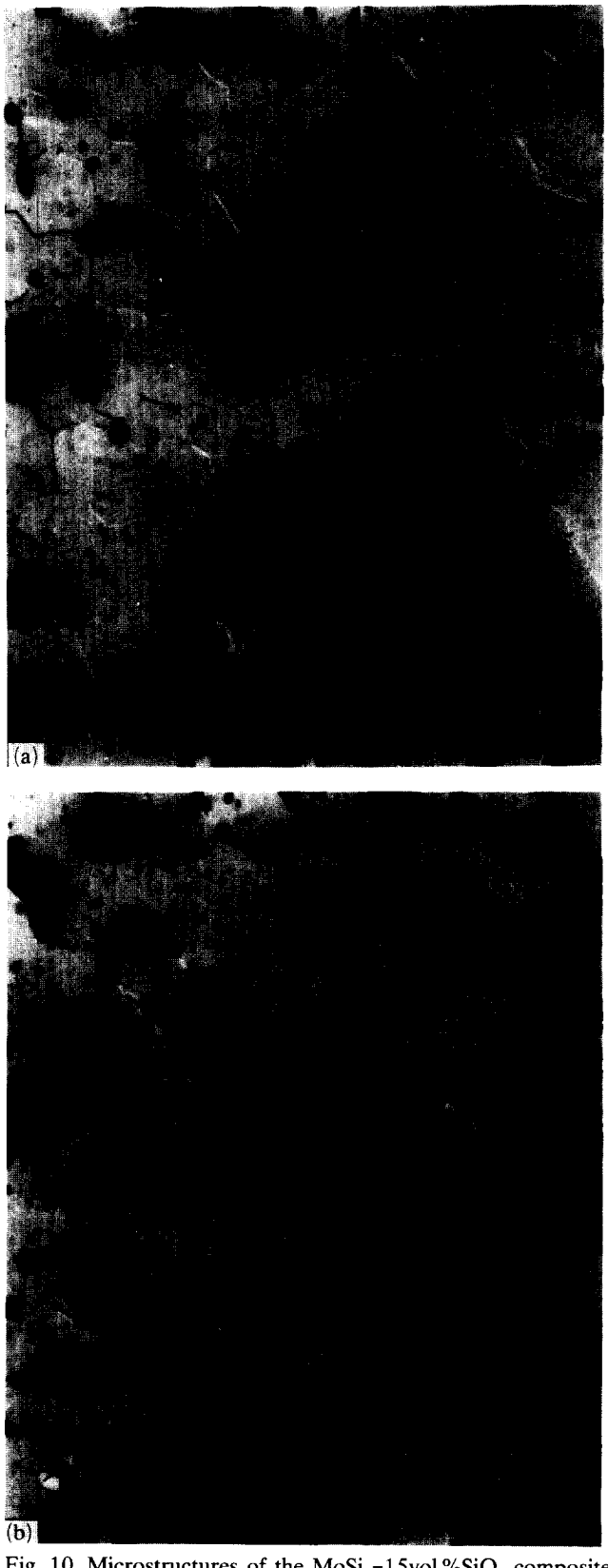

Fig. 10. Microstructures of the $MoSi_2$–15vol.%SiO_2 composite (a) before and (b) after deformation at $\dot{\varepsilon} = 10^{-4}$ s^{-1} and $T = 1200$ °C. The SiO_2 is the dark phase. Intrusion of the SiO_2 phase into the $MoSi_2$ grain boundaries is observed in (b), *e.g.* at the arrows. (a) $\varepsilon = 0$, $d = 20$ μm; (b) $\varepsilon = 0.69$, $d = 18.5$ μm.

The significant weakening caused by intentionally added SiO_2 to $MoSi_2$ is associated with its penetration of the matrix grain boundaries illustrated in Fig. 10. SiO_2 at the grain boundaries acts as a shearable film at the higher temperatures, which eases the sliding of matrix grains. This probably accounts for the $MoSi_2$ grains remaining equiaxed, even after substantial straining at 1200 °C. The present results on silica-containing $MoSi_2$ illustrate dramatically the importance of minimizing silica as a grain boundary and phase boundary contaminant during the processing of advanced $MoSi_2$-based composites for applications at temperatures above 1100–1200 °C [8].

3.4. $MoSi_2$–CaO composites

The microstructure of hot-pressed $MoSi_2$ reinforced with 20 vol.% CaO consists of equiaxed grains of $MoSi_2$ about 23–35 μm in size with smaller 1–15 μm CaO particles distributed regularly throughout the matrix, but primarily along the $MoSi_2$ grain boundaries. On deformation, severe deterioration of the particulate microstructure is observed. The matrix grains deform substantially and become slightly smaller and elongated with an aspect ratio of 1.5–2. These observations are illustrated in Fig. 11.

The results of mechanical tests for the $MoSi_2$–CaO composites in Figs. 2 and 3 do not disclose negative effects on the strength of $MoSi_2$ as does SiO_2. In fact, over much of the temperature and strain rate ranges investigated, there is a slight improvement in strength. The high CTE value of CaO compared with $MoSi_2$ is expected to lead to separation of the CaO particles from the matrix and grain boundary separation of the matrix, since the calcia is present primarily as a grain boundary phase. The general effect of CaO in both Figs. 2 and 3 appears to be modest strengthening associated with retardation of grain boundary sliding. The values of the stress exponent for the $MoSi_2$–CaO composite were obtained from Figs. 2 and 3 in the range 2–5 at both temperatures (except for the largest strain rates examined at 1100 °C, where n increases with increasing strain rate) [6] and are consistent with such analysis.

3.5. $MoSi_2$–TiC composites

TiC has potential as a toughening phase for $MoSi_2$ in the temperature regime near and above the DBTT of about 1000–1300 °C. As a monolithic material, TiC flows plastically to significant strains at these temperatures and has a relatively low DBTT of about 600 °C [9]. The plasticity can be further enhanced by decreasing the carbon content below the stoichiometry $TiC_{0.97}$. The density of TiC is relatively low (4.93 g cm^{-3}), and the CTE is nearly the same as that for $MoSi_2$. Moreover, observations to date on $MoSi_2$–TiC composites

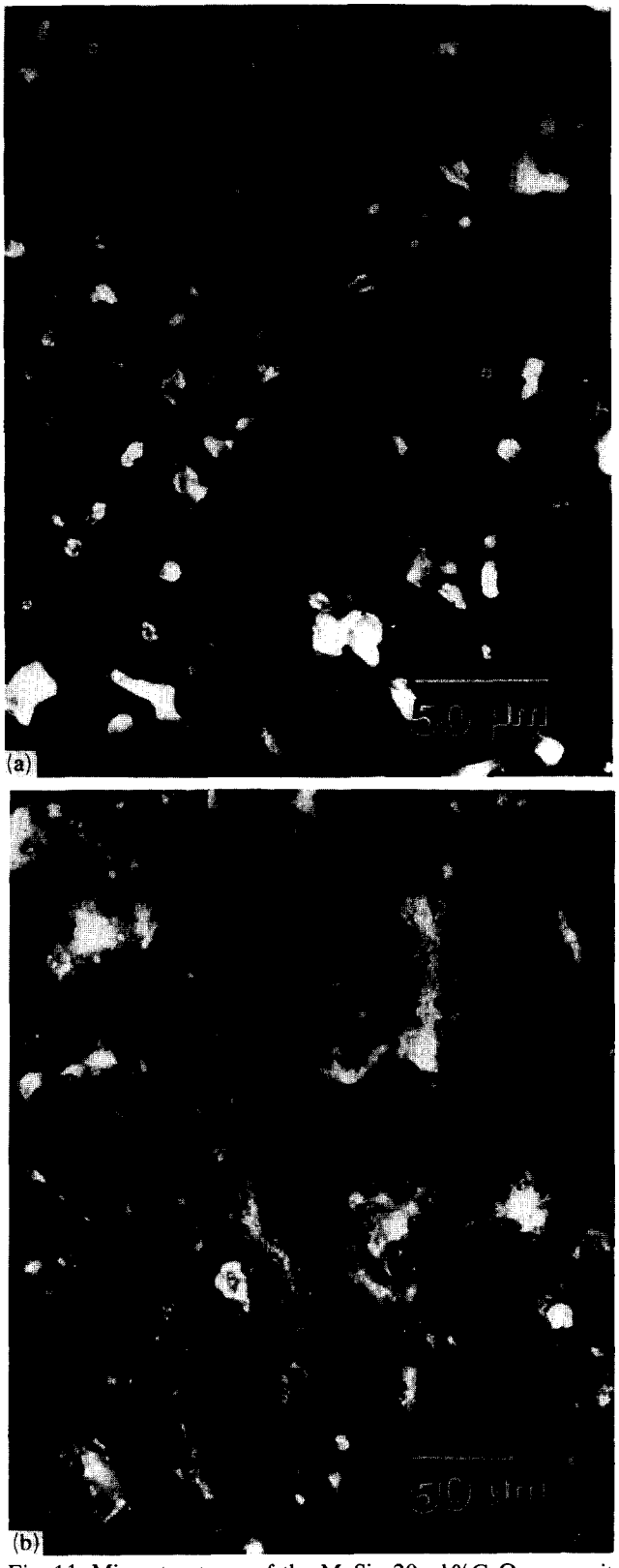

Fig. 11. Microstructures of the $MoSi_2$–20vol.%CaO composite (a) before and (b) after deformation at $\dot{\varepsilon} = 10^{-4}$ s^{-1} and $T = 1200$ °C. The CaO particles are the smaller, usually white phase in (a). Extensive plastic deformation of the $MoSi_2$ grains and fracture of CaO particles are observed in (b). (a) $\varepsilon = 0$, $d = 29$ μm; (b) $\varepsilon = 0.69$, $d = 18$ μm.

hot pressed at up to 1700 °C or heat treated extensively at 1600 °C (*e.g.* 100 h [10]) have not revealed any reaction layers or other forms of interphase instability. Our current studies have confirmed such findings for the as-processed composite, as well as after subsequent deformation at temperatures in the range 1100-1200 °C.

Figure 12 gives a representative microstructure of the as-processed composite microstructure. TiC appears as the darker phase. The interface remains intact during deformation at 1100-1200 °C, perhaps in part because a Kurdjumov-Sachs-like orientation relationship can exist between the $MoSi_2$ $C11_b$ structure and the TiC NaCl type (f.c.c.) structure. This is similar to strong interfaces observed in simpler systems such as b.c.c.-f.c.c. metallic interfaces or B_2-γ or B_2-γ' interfaces in intermetallic systems [11].

The data given in Fig. 6 illustrate the relative changes in hardness of $MoSi_2$ and TiC as a function of temperature. TiC is much harder than $MoSi_2$ at room temperature, but softens much more rapidly with increasing temperature. In the temperature range 800-1300 °C, TiC is softer and exhibits more plasticity than $MoSi_2$. Because of the higher melting temperature of TiC and perhaps because of the effects of silica-induced boundary sliding of most monolithic $MoSi_2$ materials made to date, TiC becomes harder than $MoSi_2$ at temperatures above 1300 °C.

Compression test results on the $MoSi_2$-TiC composites over the temperature range 1050-1200 °C are given in Fig. 5 and are compared with similar results for the monolithic $MoSi_2$ at two temperatures, 1150 °C and 1200 °C. The composite exhibits lower flow stresses than the monolithic material at both temperatures. At 1200 °C, the composite also exhibits greater apparent plasticity in compression. No visible cracking was noted during deformation of both materials tested at 1200 °C. At lower temperatures, all specimens exhibited cracking during deformation, and the cracking became more severe as the temperature was decreased toward 1000 °C.

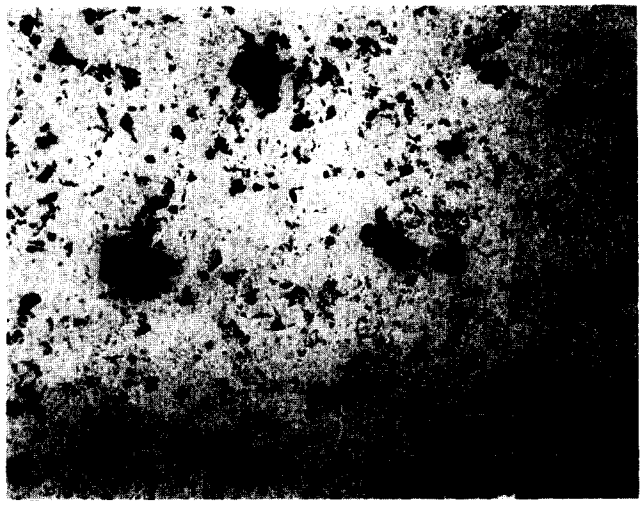

Fig. 12. Microstructures of the $MoSi_2$-10vol.%TiC composite hot pressed at 1700 °C. The TiC is the dark phase.

These results suggest that TiC might toughen $MoSi_2$ at these temperatures near the DBTT of $MoSi_2$. A possible mechanism of toughening could involve dislocation generation into the matrix phase afforded by second-phase plasticity and a favorable orientation relationship for effective slip transfer or other dislocation generation processes into the matrix. Such a mechanism has been shown to be operative in Ni-Fe-Al two-phase β-($\gamma+\gamma'$) alloys [11]. The lower relative hardness of TiC might also produce toughening by second-phase crack bridging, but at this time we have no clear evidence for the operation of any specific mechanism. Greater softening and/or toughening of the matrix may be possible through variation of the carbide volume fraction and the particle size, distribution and morphology. Additionally, improvement in processing methods to produce cleaner matrix microstructures should also allow optimization of the TiC-induced softening of $MoSi_2$ presented here in preliminary form.

3.6. Microstructural modeling

We are currently attempting to model the microstructural effects observed experimentally in Figs. 1-12 so that the important microstructural factors and physical properties that affect deformation and fracture in composites can be determined. The modeling effort also allows development of analytical methods by which the interplay of these factors can be optimized. A simple spring model description of the matrix, fiber or particle, and interface mechanics is used. Such a model allows incorporation of a wide range of microstructural features and properties into a fracture simulation experiment. The basic first-order model consists of a two-dimensional array of linear elastic springs. These springs behave linearly until they are stretched beyond a critical extension and then they break irreversibly. Microstructure can be incorporated by ascribing a different modulus (spring constant), internal stress (equilibrium spring length), and fracture energy (critical extension) to each element of microstructure. The computational approach involves applying a strain to the model microstructure, relaxing the total energy of the system, determining the maximum bond energies, finding which bonds break, and then repeating the procedure as the crack propagates.

The first-order model applies well to systems that are linear elastic and perfectly brittle, such as all four of the composite systems examined experimentally in this

paper, when they are tested at low temperatures, below the DBTT. We have applied this model to low-temperature effects of grain boundary strength on the transition between intergranular and transgranular fracture and to low-temperature fracture of script microstructures in eutectics such as those shown in Fig. 9. The results of the simulations give very good agreement with experimental results and will be reported in detail elsewhere. Such simulations allow us not only to determine values of the input parameters to obtain best agreement with experimental observations, but also to make subsequent predictions for modifying microstructural and interface properties to achieve the optimal fracture properties for these systems.

Unfortunately, many of the major problems associated with improvement of the mechanical properties of $MoSi_2$-based materials involve achievement of plastic flow in one or more microstructural element of the composite. Thus, for example, ductile-phase toughening by molybdenum or niobium in $MoSi_2$ is attempted for improvement of properties at low temperatures, and the plasticity of $MoSi_2$ and other phases (such as TiC from our current results) must be accounted for in understanding elevated temperature properties. In the present paper, we describe the results of first attempts to incorporate small-scale plasticity into the elastic mechanics model based on the two-dimensional network of springs. The extended model is initially applied to two simple microstructures—random distributions of ductile particles (molybdenum) in a brittle matrix ($MoSi_2$) and laminates or lamellar microstructures of a wide brittle layer ($MoSi_2$) and narrow ductile layers (molybdenum). Subsequent work will utilize input parameters more directly applicable to the Mo_5Si_3-, SiO_2-, CaO- and TiC-containing composites investigated experimentally in this paper. However, it should be noted that even for the computationally simple Mo-$MoSi_2$ system, the constitutive behavior (the strain to failure) for molybdenum in the simple geometries simulated is not known. Thus, it is necessary to assume a particular plasticity behavior. Even so, the initial results are encouraging.

We accomplish incorporation of small-scale plasticity into the first-order model by prescribing a non-linear force-displacement relationship for each spring. This procedure is implemented by allowing the equilibrium length of the springs to increase during plastic deformation. On unloading, only the elastic portion of the spring extensions is recovered. The present results are based upon an elastic-brittle $MoSi_2$ and an elastic-linear-hardening plastic molybdenum phase for which the $MoSi_2$-Mo interface is assumed to be very strong. In these simulations, molybdenum is modeled to have an infinite strain to fracture. Interface strength, a more realistic constitutive equation for molybdenum and other composite additions, and plasticity of the $MoSi_2$ matrix will be utilized as microstructural parameters in future simulations.

Figure 13(a) shows the simulated fracture sequence of a pre-cracked and uniaxially strained $MoSi_2$ matrix

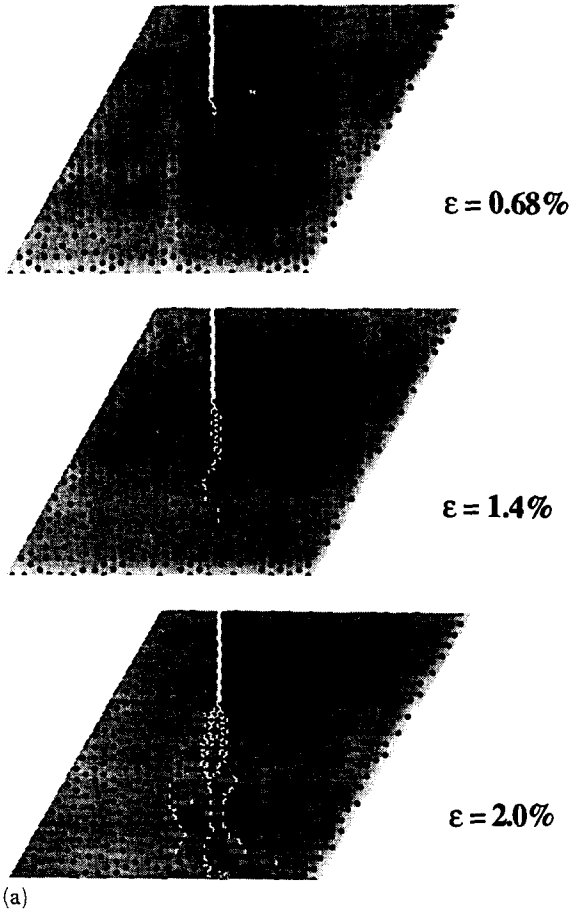

(a)

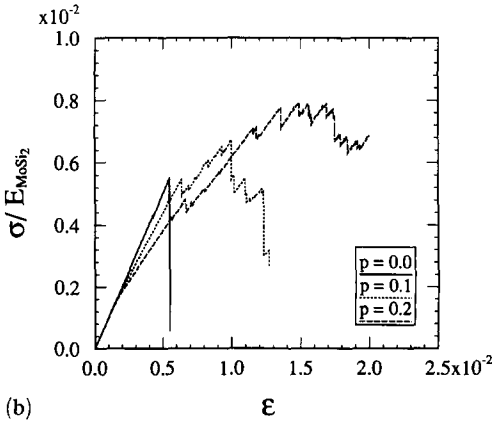

(b)

Fig. 13. (a) A fracture sequence in brittle $MoSi_2$ (gray) containing a random dispersion of 20 vol.% ductile Mo particles (black). The crack path is shown in white. The tensile stress is applied normal to the initial crack plane. (b) Stress-strain curves for pure $MoSi_2$ (——), $MoSi_2$ containing 10 vol.% ductile Mo particles (·····), and $MoSi_2$ containing 20 vol.% ductile Mo particles (- - -). p is the volume fraction.

which has been toughened by a random dispersion of 20 vol.% small molybdenum particles. The propagation of the main crack is accompanied by additional cracking in the brittle matrix as the particles intersected by the crack plastically deform. Eventually, the composite is held together by the ductile particles, which are assumed not to fracture. Figure 13(b) gives the stress–strain behavior for this composite, along with those for the unreinforced $MoSi_2$ and a composite with 10 vol.% Mo particles. The stress–strain curve for the composite continues to large strains at a slowly decreasing stress level owing to a combination of the small strain hardening coefficient assumed for the molybdenum particles and additional damage accumulation in the $MoSi_2$. Increasing the volume fraction of molybdenum particles increases both the strength and ductility of the composite, even though the yield strength of molybdenum is below the fracture strength of $MoSi_2$.

Figure 14(a) gives similar results for the simulated fracture sequence when molybdenum in the Mo–$MoSi_2$ composite is present as the ductile reinforcement of a microlaminate microstructure consisting of alternate layers of $MoSi_2$ and molybdenum, where the molybdenum layers are one quarter as thick as the $MoSi_2$ layers. These simulations apply qualitatively to the arc-melted $MoSi_2$–Mo_5Si_3 composites of Fig. 9 in which $MoSi_2$ exhibits some plasticity at 1200 °C and 1300 °C (Fig. 4). In Fig. 14(a), the microlaminate has been pre-cracked and loaded in tension parallel to the layers. The molybdenum layers are tough, and the crack propagates through the $MoSi_2$ until it reaches a molybdenum layer. The molybdenum plastically deforms, and a new crack subsequently forms in the $MoSi_2$ layer on the other side of the molybdenum layer. The crack eventually propagates through all of the $MoSi_2$ layers until the remaining load is carried predominantly by the plastically deforming molybdenum layers. Substantial damage accumulation occurs in the $MoSi_2$ immediately adjacent to the Mo–$MoSi_2$ interface because the interface is assumed to be very strong. For microlaminates, we have also performed simulations for which the Mo–$MoSi_2$ interfaces are relatively weak. In these cases, the fracture damage of the brittle phase adjacent to the interface is replaced by interfacial fracture and sliding. The stress–strain behavior for the microlaminate with the strong interface is included in Fig. 14(b), along with results for unreinforced $MoSi_2$ and a microlaminate for which the $MoSi_2$ is twice as thick. For thick $MoSi_2$ layers, the stress–strain curve shows an initial load drop due to the onset of crack propagation followed by a more substantial load drop when the crack propagates through the remaining $MoSi_2$ layers. Once all the $MoSi_2$ layers are cracked, substantial ductility is achieved owing to the plastic deformation of the molybdenum layers and the subsequent damage accumulation in the $MoSi_2$. The final fracture behavior cannot be analyzed until a better plasticity law is determined and used for the ductile layers.

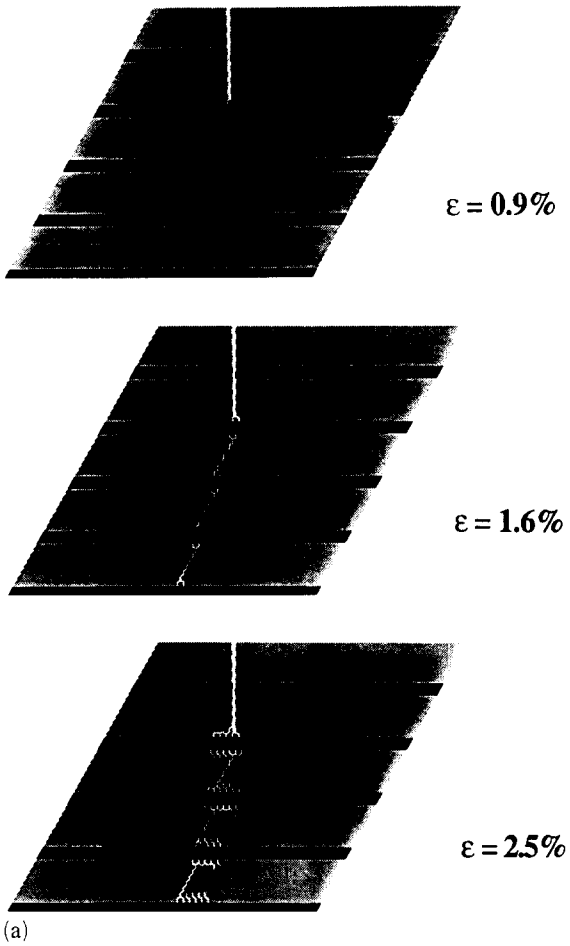

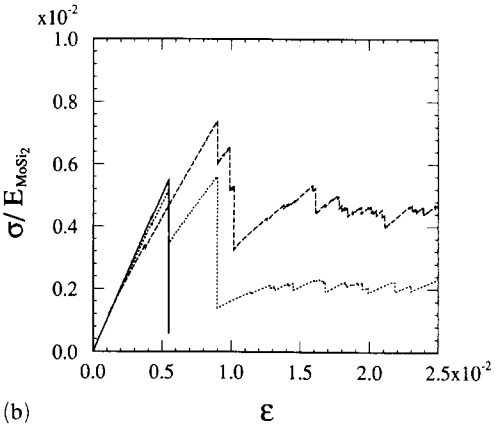

Fig. 14. (a) A fracture sequence in a $MoSi_2$ (gray)/Mo (black) microlaminate. The crack path is shown in white. The tensile stress is applied normal to the initial crack plane. (b) Stress–strain curves for pure $MoSi_2$ (——), the $MoSi_2$/Mo microlaminate of Fig. 14 (a) (– – –), and one in which the $MoSi_2$ layers are twice as wide as those in Fig. 14 (a) (· · · · ·).

4. Summary and conclusions

The deformation of $MoSi_2$ and its composites with Mo_5Si_3, SiO_2, CaO and TiC particulate reinforcements at temperatures of 1000–1300 °C and strain rates of 10^{-6}–10^{-4} s^{-1} involves contributions from dislocation creep (glide and climb) and diffusional creep processes.

For composites formed by hot pressing of powders, the addition of 15 vol.% Mo_5Si_3 to $MoSi_2$ improves the high temperature strength. Increasing the Mo_5Si_3 loading to 30 vol.% reduces the strength owing to dynamic grain refinement.

The addition of erbium to arc-melted $MoSi_2$–Mo_5Si_3 composites refines the eutectic microstructure and increases the hardness at 25–1300 °C. Crack deflection processes at 25 °C are more effective in erbium-refined microstructures than in untreated coarser eutectics.

$MoSi_2$–SiO_2 composites with coarse SiO_2 particles at $MoSi_2$ grain boundaries exhibit very poor creep resistance at high temperatures owing to low viscosity of the SiO_2 at $MoSi_2$ grain boundaries. Comparably coarse particles of CaO effect modest strengthening at the same temperatures. The very large CTE of CaO and large CTE mismatch of CaO with $MoSi_2$ may be effective in promoting strengthening of these composites, in spite of microstructural degradation associated with CaO particle disintegration.

As a composite reinforcement, TiC does not significantly interact with $MoSi_2$ and appears to cause reduced strength and some plasticity enhancement at temperatures of around 1200 °C, probably owing to dislocation pumping mechanisms at $MoSi_2$–TiC interfaces.

Microstructural modeling of the mechanical behavior of linear elastic–brittle $MoSi_2$-based composites and elastic–plastic ductile-phase toughened $MoSi_2$ has been successful in initial model system investigations. The modeling approaches will be applied more directly to the experimental results in the present investigation in future simulations.

Acknowledgments

The authors gratefully acknowledge support by the Air Force Office of Scientific Research (AFOSR) under the AFOSR URI Program, Grant No. DoD-G-AFOSR-90-0141, Dr. Alan H. Rosenstein, Program Manager. One of us (RG) also acknowledges the Los Alamos National Laboratory for a Bernd T. Matthias Fellowship during the writing of this paper.

References

1 R. M. Aikin, Jr., *Proc. 15th Ann. Conf. on Composites and Advanced Ceramics, Cocoa Beach, FL, 13–16 January, 1991,* in *Ceram. Eng. Sci., 12* (1991) 1643.
2 J. J. Petrovic and R. E. Honnell, *Ceram. Eng. Sci. Proc., 11* (1990) 734.
3 Y. Umakoshi, T. Sakagami, T. Hirano and T. Yamane, *Acta Metall., 38* (1990) 909.
4 O. Unal, J. J. Petrovic, D. H. Carter and T. E. Mitchell, *J. Am. Ceram. Soc., 73* (1990) 1753.
5 H. Kung, D. P. Mason, A. Basu, H. Chang, D. C. VanAker, A. K. Ghosh and R. Gibala, *Intermetallic Matrix Composites II*, MRS Symp. Ser., Vol. 273, Materials Research Society, Pittsburgh, PA, 1992, in the press.
6 A. Basu and A. Ghosh, *Proc. Int. Symp. on Advanced Metal Matrix Composites for Elevated Temperatures,* ASM International, Materials Park, OH, 1991, p. 41.
7 J. Major and J. Rutter, *Mater. Sci. Technol., 5* (1989) 645.
8 J. P. A. Lofvander, J. Y. Yang, C. G. Levi and R. Mehrabian, *Proc. Symp. on Advanced Metal Matrix Composites for Elevated Temperatures,* ASM International, Materials Park, OH, 1991, p. 1.
9 D. Miracle and H. Lipsitt, *J. Am. Ceram. Soc., 66* (1983) 592.
10 P. Meschter and D. Schwartz, *J. Met., 41* (11) (1989) 52.
11 M. Larsen, A. Misra, S. Hartfield-Wunsch, R. Noebe and R. Gibala, *Intermetallic Matrix Composites,* MRS Symp. Ser., Vol. 194, Materials Research Society, Pittsburgh, PA, 1990, p. 191.